ICEMG 2020-XXXXX

EKF-Based Control of FSPM Motor Supplied Through a Long Cable in ESP Application

Arta Mohammad-Alikhani[1], Abolfazl Vahedi[1], Masoud Saeidi Sharejini[1], Mehdi Rahnama[1]

[1]Iran University of Science and Technology, Tehran, Iran
Arta.alikhani@gmail.com, avahedi@iust.ac.ir, masood.saeidi.sbu@gmail.com, Mehdi.rahnama@gmail.com

Abstract
Flux switching permanent magnet (FSPM) motors are the stator-PM synchronous motors that can substitute the conventional rotor-PM motors due to their benefits in many applications such as Electrical Submersible Pumps (ESPs). Due to the long distance between the power supply set and the motor, also harsh environments in ESP for oil field applications, the signals from rotor position sensors are not reliable and therefore, a sensorless method must be employed to control the motor. Besides that, the long distance between the motor and the drive system results in the use of long cables whose impedance affects the control process and must be taken into account. Therefore, in this paper, a sensorless method based on the extended Kalman filter (EKF) is proposed for the FSPM motor which is supplied through a long cable. In order to introduce the proposed control method, the mathematical model for the FSPM motor which is series with the long cable is defined and applied to the discretized EKF. Then, the proposed method is evaluated by simulation results.
Keywords: Electrical Submersible Pump, Extended Kalman Filter, Flux switching motor, Sensorless drive.

Introduction

Traditionally, the two-pole three-phase induction motors have been used for electrical submersible pump (ESP) applications in oil wells [1]. However, over a last decade, manufactures have started to use some other motors such as interior permanent magnet (IPM) synchronous motors in ESPs, due to their advantages compared to induction motors [2]. FSPMs are the stator-PM brushless synchronous motors which have been developed in past years. The main advantages of FSPMs, as compared with conventional rotor-PM brushless motors, are favorable for cooling and high-speed operation when the motor temperature rises in poor thermal transmission [3], [4]. In addition, in rotor-PM motors, magnets usually need to be protected from the centrifugal force [5]. Therefore, for FSPM motors in which the PM is applied to the stator instead of the rotor (Fig. 1), the probability of PM fracture is almost eliminated. In FSPMs, the winding electromagnetic field is perpendicular to PM magnetic field which leads to less armature reaction effect on the PM. Thus, the less the armature reaction magnetic field effect on the PM is, the less the total demagnetizing field will be. Consequently, the probability of PM demagnetization diminishes and reliability increases.

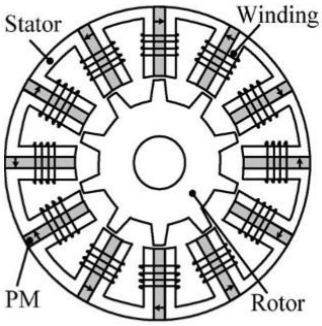

Fig. 1. The FSPM schematic. The stator contains winding and PM, and the rotor is salient pole. The stator pole number is 12 and the rotor teeth number is 10 [6].

The starting torque of this kind of motors are low and it does not have the self-starting ability. Therefore, these motors should be controlled and the Pulse Width Modulation (PWM) is used to supply them.
Most proposed control strategies for the flux switching motors in publications need the rotor position [3], [6]–[9]. In ESP systems, the motor is installed at a long distance away from the control system [10]. Due to this long distance and high noise disturbance, the signals from rotor position sensors are not reliable. Thus, a sensorless method should be applied to control flux switching motors in ESP systems in which the rotor position and speed are estimated. Some estimation methods are introduced for estimating the position and speed of the rotor in [11]. One of the appropriate methods is based on extended Kalman filter (EKF) which is appropriate for non-linear systems and less sensitive to system parameters and noise [11]. In [11,12] some method of sensorless control of AC motor are introduced, the main disadvantage of precision method is their high computational burden and complex mathematical formulas therefore According to publications, the EKF is widely proposed for the conventional synchronous PM motors [12]–[17]. In addition, in ESP systems due to the long distance, long cables must be employed to supply the motor. Long cables have impedances which cannot be ignored and therefore, result in voltage drop and error in estimation as they are not considered in the estimation method. In [18]-[21] are investigate about oilfield pump and used intelligent control method such as fuzzy logic, model predictive control and etc. However, none of the investigations for EKF consider long cables or any kind of impedances series with motors to be applied in system model in the EKF. In this article, a new method based on EKF and the field oriented control (FOC) is proposed to control the FSPM motor series with a long cable having a considerable impedance. In fact, in this strategy, only three-phase input currents are required and by measuring the currents, the rotor speed and position are estimated

by the EKF. In order to verify proposed control method, the simulations are conducted via MATLAB/Simulink and a comparison is made between the estimated and actual rotor position and speed.

The paper is structured as follows. In the next section, the EKF is introduced for state estimation; a mathematical model for the FSPM motor is represented and the model is modified for the motor along with the long cable impedance; also, the motor system is discretized and linearized for being applicable to EKF. Then, in section 3, by using the EKF, a control strategy for the FSPM motor is expressed. In section 4, simulation results are described. Finally, the last section states the conclusions derived from this work.

The EKF algorithm

The EKF is an optimal state estimator for the dynamic nonlinear systems. The design of an EKF is based on a linear approximation of the nonlinear process model. The nonlinear state equations of a system are written as follow:

$$\begin{cases} dx(t)/dt = f(x(t),u(t)) + w(t) \\ y(t) = h(x(t)) + v(t) \end{cases} \quad (1)$$

where w(t) and v(t) are the process and observation noises which are zero-mean white Gaussian noise with covariance Q(t) and R(t) respectively. The process and observation noises are independent of system states. Furthermore, *u(t)* is the input vector.

The most suitable form of the system for the process is obtained by describing motor in synchronous orthogonal two-axis dq frame. In order to get the state equations for FSPM motor, the motor dynamic equations in dq axes are described as follow:

$$\frac{d\psi_d}{dt} = u_d - Ri_d + \omega_e \psi_q \quad (2)$$

$$\frac{d\psi_q}{dt} = u_q - Ri_q - \omega_e \psi_d \quad (3)$$

In the above equations, u_d and u_q are the transformed d-axis and q-axis voltages; i_d are i_q the d-axis and q-axis currents respectively, and R is the winding resistance per phase. Considering the long cable series having resistance of R_f and inductance of L_f with the motor equations (2) and (3) becomes as

$$\frac{d\psi_d}{dt} + L_f \frac{di_d}{dt} = u_d - \left(R + R_f\right) i_d + \omega_e \psi_q \quad (4)$$

$$\frac{d\psi_q}{dt} + L_f \frac{di_q}{dt} = u_q - \left(R + R_f\right) i_q - \omega_e \psi_d \quad (5)$$

Besides, ψ_d and ψ_q are the d-axis and q-axis flux-linkage respectively which can be determined as (6) and (7). Furthermore, ω_e is the electrical rotor speed and can be expressed as (8).

$$\psi_d = L_d i_d + \psi_m \quad (6)$$

$$\psi_q = L_q i_q \quad (7)$$

$$\omega_e = P_r \omega_r \quad (8)$$

where ψ_m is the PM flux-linkage; P_r is the rotor teeth; ω_r is the angular mechanical rotor speed.

In the mathematical motor model, the angular mechanical rotor acceleration ($d\omega_r/dt$) has a relation with the electromagnetic torque (T_e), the load torque (T_L), the torque to overcome the friction and windage losses)it is assumed to be a part of load torque in this article):

$$\frac{d\omega_r}{dt} = \frac{1}{J}(T_e - T_L)$$

where *J* is the rotor inertia and T_e is given by:

$$T_e = \frac{3}{2} P_r (\psi_m i_q + (L_d - L_q) i_q i_d)$$

According to (1) to (8), and assuming

$$x = [i_d \;\; i_q \;\; \omega_e]^T \qquad u = [u_d \;\; u_q]^T \qquad y = [i_d \;\; i_q]^T$$

the system matrices *f(x,u)* and *h(x)* are resulted as (12) and (13) respectively:

$$f(x,u) = \begin{bmatrix} -\frac{(R+R_f)}{(L_d+L_f)} i_d + \omega_e \frac{1}{(L_d+L_f)} L_q i_q + u_d \frac{1}{(L_d+L_f)} \\ -\frac{(R+R_f)}{(L_q+L_f)} i_q - \omega_e \frac{1}{(L_q+L_f)} (L_d i_d + \psi_m) + u_q \frac{1}{(L_q+L_f)} \\ \frac{3}{2} \frac{P_r^2}{J} (\psi_m i_q + (L_d - L_q) i_d i_q) \end{bmatrix} \quad (12)$$

$$h(x) = \begin{bmatrix} i_d \\ i_q \end{bmatrix} \quad (13)$$

Since the load torque is incalculable for most cases, the load torque is assumed null for the system matrices. The discretised model for the FSPM motor is obtained using Euler and is defined as:

$$\begin{cases} x_{k+1} = x_k + T_s\left(f(x_k, u_k)\right) + \sigma_k \\ y_k = h(x_k) + \lambda_k \end{cases} \quad (14)$$

where $x_{k+1} = x\left(\left[k+1\right]T_s\right)$, $x_k = x\left(kT_s\right)$; T_s is the sample-time.

In the EKF, the estimated state vector $\hat{x}_{k|k}$ and its covariance matrix $P_{k|k}$ are obtained through two steps. In the first step, a prediction for $\hat{x}_{k|k-1}$ and also $P_{k|k-1}$ is performed as (15) and (16) respectively.

$$\hat{x}_{k|k-1} = \hat{x}_{k-1|k-1} + T_s f(\hat{x}_{k-1|k-1}, u_{k-1}) \quad (15)$$

$$P_{k|k-1} = P_{k-1|k-1} + T_s (F_{k-1} P_{k-1|k-1} + P_{k-1|k-1} F_{k-1}^T) + Q \quad (16)$$

In the second step, the predicted state and its covariance matrix will be corrected and updated accordingly to (17) and (18).

$$\hat{x}_{k|k} = \hat{x}_{k|k-1} + K_k(y_k - h(\hat{x}_{k|k-1})) \quad (17)$$

$$P_{k|k} = P_{k|k-1} - K_k H P_{k|k-1} \quad (18)$$

The matrices *F* and *H* are the Jacobian matrices for *f(x,u)* and *h(x)* respectively and given by (19) and (20). The filter gain matrix K_k is defined by (21).

$$H = \left.\frac{\partial h(x)}{\partial x}\right|_{x_{k|k-1}} = \begin{bmatrix} 1 & 0 & 0 \\ 0 & 1 & 0 \end{bmatrix} \quad (20)$$

$$K_k = P_{k|k-1} H^T (H P_{k|k-1} H^T + R)^{-1} \quad (21)$$

In order to estimate the state according to above procedure, the Jacobian matrix must be calculated each iteration. The estimation of the rotor position can be carried out by integrating the estimated speed as

$$\theta_{ek+1} = \theta_{ek} + T_s \omega_e \quad (22)$$

The proposed control strategy

The block diagram of a sensorless FOC system for the flux-switching motor is shown in Fig. 2. It comprises three proportional-integral (PI) regulators, the EKF block for the speed estimation purpose, and a sinusoidal PWM (SPWM) generator. Two of the PI regulators are used to force the electric current in both phases d and q to reach their desired values, whereas the third regulator is used to regulate the motor speed. As it depicted in Fig. 2, at the input, the PI speed regulator compares speed reference ω_e^* with estimated speed $\hat{\omega}_e$ and it delivers as output reference q axis current i_q^*. The other two PI controllers compare the two diagonal *dq* axes currents with the reference one. In order to obtain maximum torque to current ratio, the reference current for the i_d^* is kept zero [23]. The PI regulators outputs are transformed to the ABC frame using the estimated rotor position θ_e. The transformed outputs are delivered to the SPWM generator. The PWM which is generated by SPWM method is delivered to the inverter which supplies the motor.

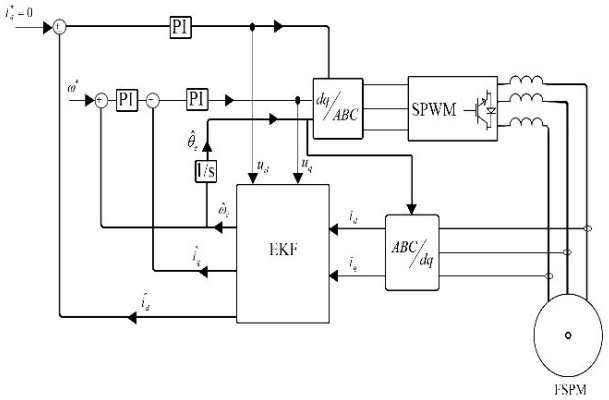

Fig. 2. The proposed sensorless drive system.

$$F(x(t)) = \left.\frac{\partial f(x,u)}{\partial x}\right|_{x_{k-1|k-1}} = \begin{bmatrix} -\frac{R+R_f}{L_d+L_f} & -\frac{1}{L_d+L_f}L_q\omega_e & \frac{1}{L_d+L_f}L_q i_q \\ \frac{1}{L_q+L_f}L_d\omega_e & -\frac{R+R_f}{L_q+L_f} & -\frac{1}{L_q+L_f}(\psi_m + L_d i_d) \\ \frac{3}{2}\frac{P_r^2}{J}((L_d-L_q)i_q) & \frac{3}{2}\frac{P_r^2}{J}(\psi_m + (L_d-L_q)i_d) & 0 \end{bmatrix} \quad (19)$$

The EKF uses i_d, i_q, u_d, and u_q as input and delivers i_d, i_q, and ω_e at the output as the estimated states. The inputs i_d and i_q are obtained by transformation the measured ABC currents to $d-q$ frame. In addition, the inputs u_d and u_q are taken from the PI regulators output as it depicted in Fig. 2. Therefore, by using the data from the PI output there will be no need to voltage sensors.

Results and Discussion

To verify the proposed sensorless control strategy, the FSPM motor with Table I parameters series with the long cable is developed along with the control system in MATLAB/Simulink as Fig. 3. The cable parameters are supposed to be $R = 6.2\Omega$ and *L*=2mH where the cable length is 5 km. In the case study, it is assumed that the load torque has a relation with the square value of mechanical rotational speed ω_r as (23). Hence, the load torque at the rated speed (3000 *rpm*) is 101.86 *Nm*.

$$T_L = 0.001032\,\omega_r^2 \quad (23)$$

TABLE I
THE PARAMETER OF THE FSPM MOTOR

The FSPM motor parameters	Value
Rated Voltage of Phase (*V*)	1000
Rated current (*A*)	12.6
Stator teeth number	12
Rotor teeth number	10
Phase resistance (Ω)	0.8266
PM flux-linkage (*Wb*)	0.388
d-axis inductance (*mH*)	8.14
q-axis inductance (*mH*)	9.07
Rotational inertia ($kg.m^2$)	0.0085
Rated torque (*Nm*)	102

Rated speed (*rpm*)	3000

Choosing the values of matrices R, Q and P_0 is performed with a trial-and-error to reach stability and shorter convergence time. The R, and P_0 is as (24).

$$Q = \begin{bmatrix} 0.5 & 0 & 0 \\ 0 & 5 & 0 \\ 0 & 0 & 10^5 \end{bmatrix}$$
$$R = \begin{bmatrix} 50 & 0 \\ 0 & 50 \end{bmatrix} \qquad (24)$$
$$P_0 = \begin{bmatrix} 1 & 0 & 0 \\ 0 & 1 & 0 \\ 0 & 0 & 10^3 \end{bmatrix}$$

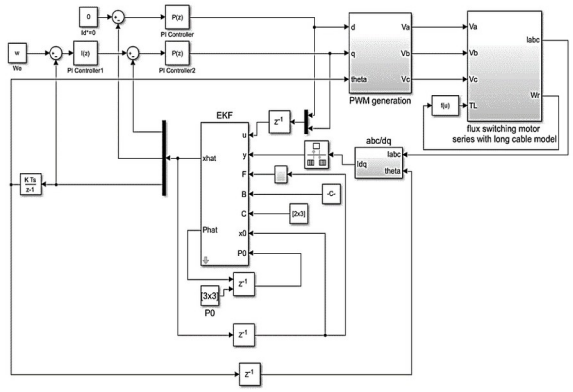

Fig. 3. The developed model of the proposed control system along with motor series with the long cable in MATLAB/Simulink.

The initial value of covariance matrix P_0 influences less than the other matrices in the initial tuning procedure of the Kalman filter [12]. Since the motor starts from the standstill condition, the initial state vector has been considered the null vector.

The regulators coefficients are also chosen by trial-and-error for the soft-starting purpose. The values are kept unchanged for all simulation cases.

Fig. 4. depicts the motor actual speed for the cases with reference speed equal to 3000 *rpm*, 2500 *rpm*, 2000 *rpm*, and 1500 *rpm*. The results show that the motor controlled by the proposed method has the appropriate response in the ranges of speed. The phase A current for the reference speed equals to 3000 *rpm* is illustrated in Fig. 5. The current gradually increases and after 1 second reaches around 17.8 *A* and the root mean square of the current is around 12.6 *A*. This means that the voltage drop due to the long cable is about 78.7 *V*. The estimated and actual rotor electrical position of the motor are demonstrated in Fig. 6 in which a small interval of steady state is chosen to be shown. According to Fig. 6, at steady state, the estimated and actual rotor position are mostly coincident which shows that the estimation is performed accurately.

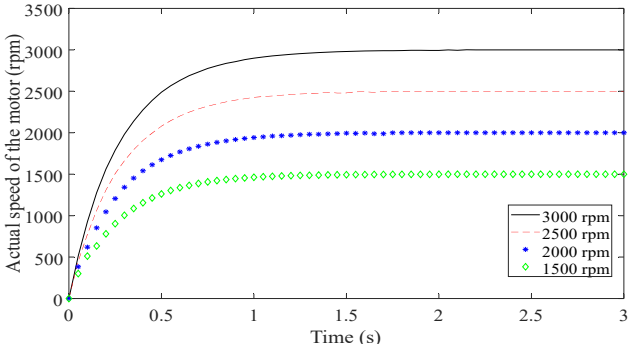

Fig. 4. Speed trajectory for some reference speed from 1500 rpm up to 3000 rpm.

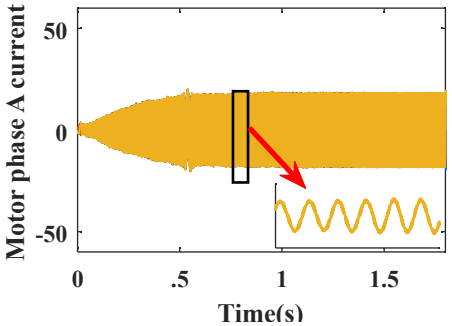

Fig. 5. The current of phase A for the reference speed 3000 rpm case.

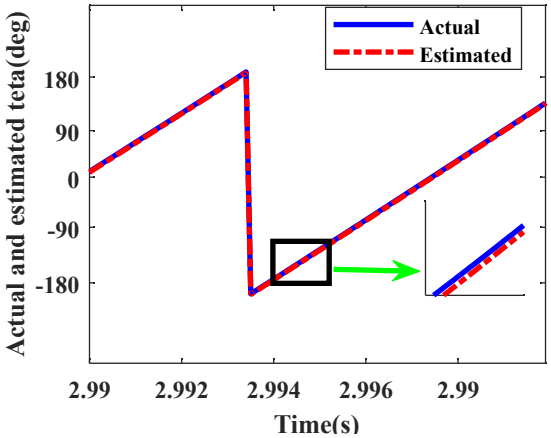

Fig. 6. The estimated and actual rotor electrical position at a small time interval in steady state for the reference speed 3000 *rpm* case.

In Fig. 7, the electromagnetic torque of the motor for the reference speed 3000 *rpm* is represented. It is obvious that before the moment t=2.1 second, the torque has considerable ripple and after the moment at steady state the ripple diminishes and settles to about 4 percent similar to the estimated speed in which the ripple before the steady state is considerable and that is because of continuous load change before steady state (Fig. 8). After the steady state the ripple of estimated speed decreases and speed estimation is performed well by the EKF which is obvious form Fig. 8.

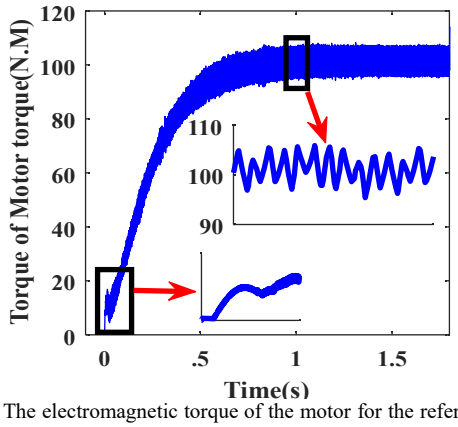

Fig. 7. The electromagnetic torque of the motor for the reference speed 3000 *rpm* case.

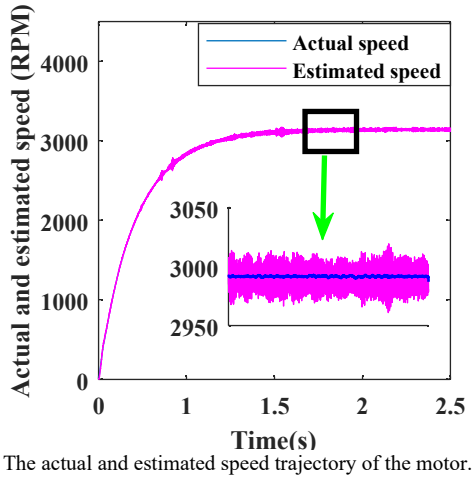

Fig. 8. The actual and estimated speed trajectory of the motor.

Fig. 9 illustrates the motor speed when a sudden change in load torque occurs at t=3s. In this case, the load torque is increased 20 *Nm* and reached to 121.85 *Nm* at this moment. Despite load torque sudden increment at the moment 3 second, it becomes less than 121.85 *Nm* as to the speed 54 *rpm* reduction and the speed decreases to 2946 *rpm* which eventually reaches 3000 *rpm* within 1 seconds.

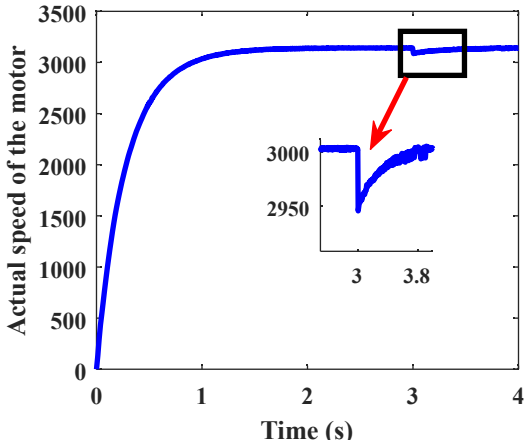

Fig. 9. The speed trajectory for the case of the sudden 20 Nm increment in load torque.

Deceleration model is one of the main case studied in electric drive and is important in regenerative mode control therefore in this paper investigate FSPM motor deceleration mode. In this case study motor speed set point in t=2.5 (s) suddenly change to 0 from 3000 rpm. Simulation result is showed that measurement speed is decrees and reach to near 0 rpm with low steady state. Simulation result is shown in Fig (10).

Conclusions

In this paper, a novel sensorless method base on EKF has been proposed for the control of the FSPM motor series with the long cable in ESP systems. The mathematical model of the motor which is applied to EKF has been modified to take the long cable into account. The control strategy uses the estimated speed obtained by EKF through two steps and the electrical position of the rotor that is the discrete integration of estimated speed. Simulations indicate that the discrepancy between estimated and actual electrical position of the rotor is insignificant. On the other hand, the motor performs well in the speed range of 1500 rpm to 3200 rpm. The Results show that the method has a good response to sudden change in load torque. Therefore, the control method is applicable for many applications that use FSPM motors.

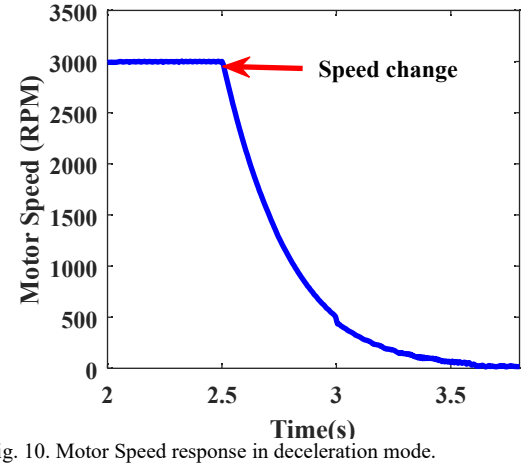

Fig. 10. Motor Speed response in deceleration mode.

References

[1] T. R. Brinner, R. H. McCoy, and T. Kopecky, "Induction Versus Permanent-Magnet Motors for Electric Submersible Pump Field and Laboratory Comparisons," *IEEE Transactions on Industry Applications*, vol. 50, no. 1, pp. 174–181, Jan. 2014.

[2] S. F. Rabbi, M. A. Rahman, and S. D. Butt, "Modeling and operation of an interior permanent magnet motor drive for electric submersible pumps," in *2014 Oceans - St. John's*, 2014, pp. 1–5.

[3] H. Jia, M. Cheng, W. Hua, W. Lu, and X. Fu, "Investigation and Implementation of Control Strategies for Flux-Switching Permanent Magnet Motor Drives," in *IEEE Industry Applications Society Annual Meeting*, 2008, pp. 1–6.

[4] M. H. B. Bafghi, A. Vahedi, A. M. Alikhani, and N. Takorabet, "Shaft twisting effect on steady state performance of flux switching motor with long rotor," *International Journal of Applied Electromagnetics and Mechanics*, vol. Preprint, no. Preprint, pp. 1–13, Apr. 2019.

[5] M. Cheng, W. Hua, J. Zhang, and W. Zhao, "Overview of Stator-Permanent Magnet Brushless Machines," *IEEE Transactions on Industrial Electronics*, vol. 58, no. 11, pp. 5087–5101, Nov. 2011.

[6] W. Zhao *et al.*, "Stator-Flux-Oriented Fault-Tolerant Control of Flux-Switching Permanent-Magnet

Motors," *IEEE Transactions on Magnetics*, vol. 47, no. 10, pp. 4191–4194, Oct. 2011.

[7] Y. Gu, L. Quan, and Z. Xiang, "Minimization the torque ripple of flux-switching permanent magnet motor based on iterative learning control," in *2014 17th International Conference on Electrical Machines and Systems (ICEMS)*, 2014, pp. 1985–1989.

[8] Pengfei Zhou, Yu Wang, and Zhiquan Deng, "A torque impulse balance control method to achieve optimal dynamic response for permanent magnet flux-switching motor," in *2014 IEEE Conference and Expo Transportation Electrification Asia-Pacific (ITEC Asia-Pacific)*, 2014, pp. 1–5.

[9] W. Zhao, M. Cheng, W. Hua, H. Jia, and R. Cao, "Back-EMF Harmonic Analysis and Fault-Tolerant Control of Flux-Switching Permanent-Magnet Machine With Redundancy," *IEEE Transactions on Industrial Electronics*, vol. 58, no. 5, pp. 1926–1935, May 2011.

[10] M. Smochek, A. F. Pollice, M. Rastogi, and M. Harshman, "Long Cable Applications From a Medium-Voltage Drives Perspective," *IEEE Transactions on Industry Applications*, vol. 52, no. 1, pp. 645–652, Jan. 2016.

[11] Y. Li and H. Zhu, "Sensorless control of permanent magnet synchronous motor - a survey," *Vehicle Power and Propulsion Conference, 2008. VPPC '08. IEEE*, pp. 1–8, 2008.

[12] S. Bolognani, R. Oboe, and M. Zigliotto, "Sensorless full-digital PMSM drive with EKF estimation of speed and rotor position," *IEEE Transactions on Industrial Electronics*, vol. 46, no. 1, pp. 184–191, 1999.

[13] R. Dhaouadi, N. Mohan, and L. Norum, "Design and implementation of an extended Kalman filter for the state estimation of a permanent magnet synchronous motor," *IEEE Transactions on Power Electronics*, vol. 6, no. 3, pp. 491–497, Jul. 1991.

[14] A. Qiu, Bin Wu, and H. Kojori, "Sensorless control of permanent magnet synchronous motor using extended Kalman filter," in *Canadian Conference on Electrical and Computer Engineering 2004 (IEEE Cat. No.04CH37513)*, pp. 1557–1562.

[15] Y. Shi, K. Sun, L. Huang, and Y. Li, "Online Identification of Permanent Magnet Flux Based on Extended Kalman Filter for IPMSM Drive With Position Sensorless Control," *IEEE Transactions on Industrial Electronics*, vol. 59, no. 11, pp. 4169–4178, Nov. 2012.

[16] S. Bolognani, L. Tubiana, and M. Zigliotto, "Extended kalman filter tuning in sensorless PMSM drives," *IEEE Transactions on Industry Applications*, vol. 39, no. 6, pp. 1741–1747, Nov. 2003.

[17] N. K. Quang, N. T. Hieu, and Q. P. Ha, "FPGA-Based Sensorless PMSM Speed Control Using Reduced-Order Extended Kalman Filters," *IEEE Transactions on Industrial Electronics*, vol. 61, no. 12, pp. 6574–6582, Dec. 2014.

[18] D. Janiszewski, "Extended Kalman Filter Based Speed Sensorless PMSM Control with Load Reconstruction," in *IECON 2006 - 32nd Annual Conference on IEEE Industrial Electronics*, 2006, pp. 1465–1468.

[19] N. Mohan, "Advanced Electric Drives Analysis, Control, and Modeling using MATLAB-Simulink," *Wiley*, vol. 1, 2015.